analytical chemistry

Article

pubs.acs.org/ac

Particle Tracking and Multispectral Collocation Method for Particle-to-Particle Binding Assays

Anita Rogacs and Juan G. Santiago*

Department of Mechanical Engineering, Stanford University, Stanford, California 94305, United States

Supporting Information

ABSTRACT: We present a simple-to-implement method for analyzing images of randomly distributed particles transported through a fluidic channel. We term this method particle imaging, tracking and collocation (PITC). Our method uses off-the-shelf optics including a CCD camera, epifluorescence microscope, and a dual-view color separator to image freely suspended particles in a wide variety of microchannels (with optical access for image collection). The particles can be transported via electrophoresis and/or pressure driven flow to increase throughput of analysis. We here describe the implementation of the algorithm and demonstrate and validate three of its capabilities: (1) identification of particle coordinates, (2) tracking of particle motion, and (3) monitoring of particle interaction via collocation analysis. We use Monte Carlo simulations for validation and optimization of the input parameters. We also present an experimental demonstration of the analysis on challenging image data, including a flow of two, interacting Brownian particle populations. In the latter example, we use PITC to detect the presence of target DNA by monitoring the hybridization-induced binding between the two populations of beads, each functionalized with DNA probes complementary to the target molecule.

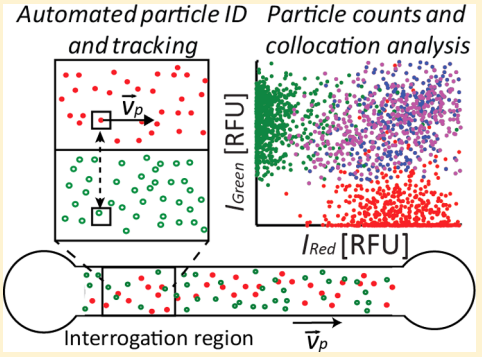

Accompanying the growing number of particle, cell, and bead-based assay applications,[1−6] particle and cell analysis methods have become more rigorous and sophisticated.[7,8] The two most frequently cited techniques are likely flow-cytometry (FCM)[8,9] and laser-scanning cytometry (LSC).[10] Flow cytometry is a workhorse technology used routinely in immunology,[11] pathology,[12] and hemotology.[13] FCM performs a single high content multiparametric measurement for thousands of particles in minutes or less. (We shall use "particles" to denote living and fixed cells or micrometer-scale fluorescent beads such as Luminex beads[14,15]) The core of a standard cytometer is a flow chamber where a particle-laden stream is hydrodynamically focused with the aid of sheath flow into a small interrogation region through which particles traverse one at a time. Lasers illuminate particles in the interrogation region. Forward light scatter is approximately correlated to the size of the particle and side scatter contains particle granularity information.[9] Increasing need for multiplexing via polychromatic excitation and emission has pushed the frontiers of flow cytometry, and enabled, for example, implementation of instruments that measure up to 19 parameters (17 fluorescent colors and 2 physical parameters).[11]

LSC[10] was originally designed to provide an imaging complement to traditional FCM and allow morphological analysis of adherent cells.[16] LSC scans stationary particles (typically cells) adhered to a surface and its implementation has evolved to include analyses of cell proliferation, tissue architecture, and immunophenotyping using precious samples.[2] The cells are fixed onto slides and scanned with multiple lasers. This can be repeated over time for studies of enzyme kinetics and other time-resolved processes. The slide can be removed from the instrument to change staining or otherwise modify the cells; and then placed back on the instrument for reanalysis.[16] Each cell can be relocated and all data points can be correlated for multivariate analysis.

There is a range of other multicolor particle image counting and analysis systems. For example, recently the field has seen the development of imaging versions of FCM systems wherein point detectors are replaced by high speed imaging to analyze particle morphology in more detail and using up to 12 wavelengths (e.g., the Amnis Imagestream system). These systems employ time delay integration (TDI) wherein the particle-specific detection region of the camera is panned electronically to track the cells in the flow stream. These systems can produce up to 12 simultaneous realizations of a darkfield, two brightfield images, and nine fluorescence images of each particle in suspension.

In this work, we present a simple-to-implement alternative technology for multispectral particle enumeration, image analysis, collocation and quantitation of particle-to-particle interactions. Our method is applicable for either single images or sequential-in-time images of randomly distributed particles flowing in a channel. Our method identifies, and tracks hundreds of particles simultaneously and offers measurements of fluorescence intensity, particle image size, and collocation

Received: September 6, 2013
Accepted: November 13, 2013

dx.doi.org/10.1021/ac402830q | *Anal. Chem.* XXXX, XXX, XXX−XXX

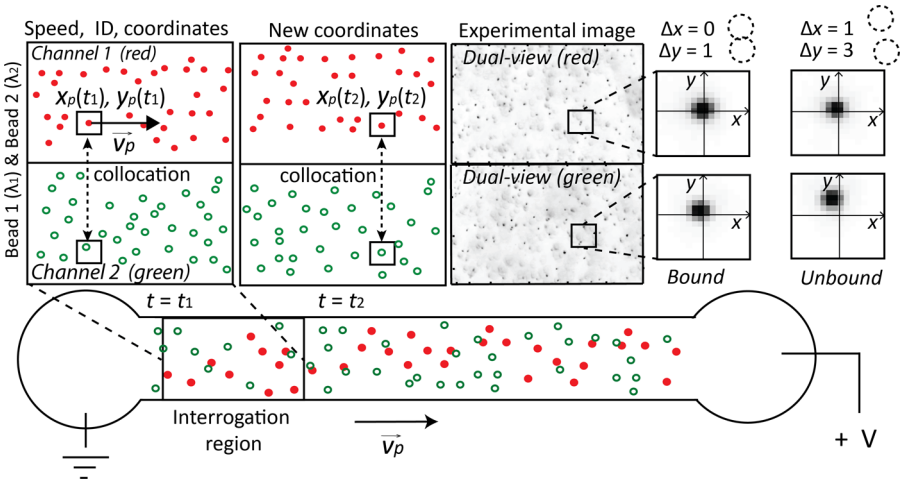

Figure 1. Particle imaging, tracking and collocation for particle monitoring and particle-to-particle binding assays. A two-color version is shown here, but the system is easily scalable to four colors using off-the-shelf instrumentation. A typical experiment involves (1) loading a solution containing particles emitting in the red and green into a microchannel; (2) electrophoresing the particles through a detection region with optical access; and (3) imaging at a user-specified rate using a microscope equipped with dual-view system and high-sensitivity CCD camera. The dual-view system chromatically separates the particle images into separate spatial domains on the CCD array. The PITC algorithm determines location and in-plane velocity vectors of each particle in one spectral channel. This analysis is used to track the coordinates, image size, and fluorescence intensity of the individual particles in time. The subregions surrounding the particles in channel 1 are identified and tracked then cross-correlated with the corresponding subregions in the other channel. The persistence (in time) of a high cross-correlation signal indicates deterministically bound particles.

between multiple colors. The latter helps monitor particles, which emit at multiple wavelengths and particle-to-particle type interactions. One unique feature of our technique is that it can monitor the time evolution of particle−particle interactions (we demonstrate evolution times of ∼8 s, but this can be increased by changing flow or imaging conditions). Further, our image analysis can handle suspensions with particle densities in excess of 10^8 mL^{-1} (by comparison, FCM require densities of 10^6 mL^{-1} or less). All of the analysis can be performed on a particle suspension inside virtually any microchannel or tube with optical access for particle imaging, including off-the-shelf microfluidic chips. In comparison, FCM and LSC systems each require specialized particle handling systems: Precise hydrodynamic focusing for FCM and immobilization and scanning for LSC. Here we demonstrate a version of our technique optimized for analyzing specific particle-to-particle interactions and the resulting collocation and correlation of particle image motions.

MATERIALS AND METHODS

Overview of Collocation Method. The example setup of our PITC method uses a standard epifluorescence microscope with a 20× objective, a CCD camera equipped with a dual-view color separator,[17] and a mercury arc lamp for illumination. The particles are suspended in an aqueous solution and loaded onto a microfluidics chip, as depicted schematically in Figure 1. The particles are transported through the interrogation region via electrophoresis. Our instrumentation is simple and off-the-shelf; and we rely instead on image analyses and computations for detailed analysis. Our custom particle tracking algorithm tracks each particle and monitors its location, size, diffusivity, fluorescence intensity, and its correlation to particle images at other wavelengths in time. Our technique can generate time-resolved measurements for thousands of particles in minutes.

Reagents and Materials. We purchased yellow-green (505/515) and crimson-red (625/645), 1.0 μm carboxylate-modified fluorescent polystyrene microbeads, (FluoSpheres, Molecular Probes, Life Technologies). Note that the extinction coefficient for polystyrene in the wavelength range of 0.3−1.2 μm is less than 10^{-5}.[18] Particles are therefore approximately transparent to the excitation and emission wavelengths, so that overlapping of two particles along the optical axis is not expected to result in significant signal attenuation due to absorption. The beads were conjugated with amine labeled complementary DNA probes by Radix Biosolutions. Conjugated beads were mixed with target DNA (See Supporting Information, SI, for sequence information) in a buffer containing 20 mM Tris, 10 mM hydrochloric acid, HCl, 0.08% Triton X-100 and 50 mM sodium chloride, NaCl. Reagents Tris, HCl, Triton X-100, and NaCl were purchased from Sigma-Aldrich (St. Louis, MO). The DNA was synthesized by Integrated DNA technologies, (IDT, Coralville, IA) and was desalted or PAGE purified (See SI, Section S.9). The buffered bead suspension was first mixed with 100 nM target DNA in presence of 3×10^9 beads/mL of each color and incubated at 60 °C for 1 min followed by 50 °C incubation for 10 min. The solution was diluted 10-fold with the hybridization buffer and pressure loaded into a poly(methyl methacrylate) microfluidic chip channel with dimensions 2 × 0.15 × 100 mm (SI Figure S.6). The output well was filled with 50 μL of 1 M Tris-HCl buffer. The loading well was filled with the same buffer containing 25% Pluronic F-127 solution in order to reduce pressure driven flow (see SI section S.10 for loading protocol). Platinum electrodes were placed in the loading and output wells and electrophoresis was initiated by applying a constant current of 100 μA. The bead suspension is imaged using an Olympus IX70 microscope equipped with a 20×, NA = 0.5 Olympus UPlanFl objective, a 16-bit CCD (Cascade 512F) camera (520 × 520 of 16 μm pixels). The optical depth of field of the microscope objective is 3.8 μm (evaluated at λ = 550 nm).[19] The characteristic depth of the particle tracking measurement volume is 11.5 μm (at λ = 550 nm).[20] The focal plane was placed about halfway between the bottom and top

dx.doi.org/10.1021/ac402830q | Anal. Chem. XXXX, XXX, XXX−XXX

walls of our chip. Our 150 μm by 275 μm field of view was roughly centered along the spanwise 2 mm width of the channel. We achieved spatial separation of two wavelengths using an XF53 dual pass filter cube (Omega Optical) with peak excitation wavelength ranges of 475−500 and 550−600 nm, and peak emission wavelength ranges of 500−550 and 600−675 nm, in combination with a quad-view imager (MicroImager, Photometrics, Tucson, AZ). In a typical experiment, we record 200 images of particles illuminated with a mercury light source for 5 ms at a frequency of 1 Hz. During this time, on the order of 1000−10 000 unique beads traverse through the field of view. The particle motion and imaging rate can be increased for applications requiring higher throughput and where particles or cells require shorter monitoring times.

Particle Tracking and Collocation Algorithm. Figure 2 shows an overview of our PITC algorithm, which we implemented on MATLAB (Mathworks Inc., Natick, MA). The schematic displays the core phases of the PITC algorithm and their corresponding output parameters. In section S.2 of SI we include detailed description of the implementation and the list of input and output parameters of these core PITC phases. To summarize briefly, we first spatially register the two spectral channels using a bright field image of an alignment mask (see SI section S.2.1). The algorithm is then divided into two phases. In the first phase, we analyze particle images from one spectral channel (Channel 1) to identify and track particle coordinates, size and fluorescence (see SI section S.2.2). In the second phase, we perform collocation, which analyzes regions in the second channel images (Channel 2) which are immediately near particles identified in the first channel (see SI section S.2.3). The process can be performed twice with the first phase starting with each of the two channels. This enables counting and tracking particles individually in each channel and corroboration of the collocation analysis. For the current demonstration, the algorithm is performed as a postprocess routine but the process is amenable to parallelization and real-time implementation.

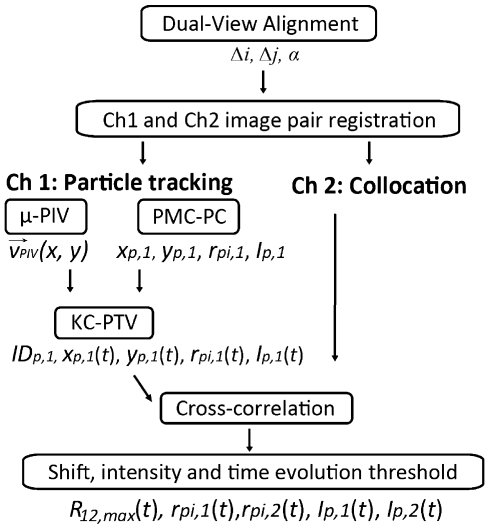

Figure 2. PITC algorithm structure. Each image sequence contains data for thousands of unique particles. After registration of the two images, the algorithm proceeds in two main phases. The first phase quantifies local drift particle velocities using micrometer resolution particle image velocimetry (micro-PIV). Unique particle images in Channel 1 (Ch1) are then identified, located and characterized via the particle mask correlation and particle characterization (PMC-PC) method. The particle image intensity and radius are evaluated using a nonlinear Gaussian fitting routine. The algorithm then combines results of PMC-PC and micro-PIV for a particle tracking velocimetry (PTV) subroutine enhanced by Kalman filter and χ^2-testing method (KC-PTV). This analysis results in accurate determination and tracking of the location of each particle over time and space. The second phase of the algorithm cross-correlates subregions surrounding the particle locations identified in Ch1 with corresponding subregions in the registered Ch2. Ch2 particle characteristics, such as radius and total fluorescence, are evaluated using the Gaussian fitting subroutine. Thresholds for intensity, size, velocity, and correlation coefficient are applied at each step to eliminate spurious results. For more details, see S.2 of SI.

Particle Monitoring Time to Discriminate Bound Particles. Our algorithm relies on particle brightness patterns, and so we recommend imaging conditions such that particle image diameters correspond to distances of 3 or more pixels (roughly 3−8 pixels is ideal). To discriminate between bound and closely neighboring particles we can monitor the persistence (in time) of the spatial correlation of particle images. This option places a minimum requirement on the amount of time the algorithm tracks particles. The algorithm should track particles long enough for Brownian motion or other dispersion to cause separation of unbound particles. For particle separation phenomena determined by Brownian motion, we can estimate this minimum time of observation from particle diffusivity. For particles with radius, r_p, and particle image radius (geometrically projected into the object plane), r_{pi}, we recommend the following relation to estimate the minimum time, t_{ch}, over which to track particle pairs undergoing Brownian diffusion:

$$L_{ch} = \sqrt{4D_{eff}t_{ch}} > [(r_{p,1} + r_{p,2}) + (5/4)\min(r_{pi,1}, r_{pi,2})] \quad (1)$$

Here, L_{ch} is a characteristic minimum particle center-to-center distance in object space required before the algorithm concludes the particles are not bound. At the characteristic time, t_{ch}, diffusion statistics[21] suggest that 67% of all randomly aligned particles pairs with effective diffusivity of D_{eff}, are separated by L_{ch}. We estimate the Brownian separation distance between two particles using an effective diffusion coefficient of the form $D_{eff} = D_{p1} + D_{p2}$, where D_{p1} and D_{p2} are respectively the diffusivities of particles imaged in channels 1 and 2. Here we assume that the diffusive motions of the closely spaced particles are statistically independent.[21] (See section S.3 of SI for more details.) Combining eq 1 with the Einstein diffusivity expression,[22] $D_P = 2kT/3\pi\mu r_p$, we can solve for the characteristic minimum evolution time:

$$t_{ch} = \frac{3\pi\mu((r_{p,1} + r_{p,2}) + (5/4)\min(r_{pi,1}, r_{pi,2}))^2}{2kT\left(\frac{1}{r_{p,1}} + \frac{1}{r_{p,2}}\right)} \quad (2)$$

In our experiments, this time is roughly 2.5 s. Appropriate choices for monitoring time are discussed further in the Validation and Performance section.

Interpreting Collocation Data. The persistence (in time) of a high cross-correlation signal indicates deterministically bound particles. This is in contrast to unbound, but closely neighboring particles, which eventually separate due to Brownian motion and/or dispersion. We identify particles as bound only if their collocation coefficient $R_{12,max}(t)$ remains sufficiently high for longer than a predefined minimum tracking

dx.doi.org/10.1021/ac402830q | Anal. Chem. XXXX, XXX, XXX−XXX

time, t_{ch}, determined from eq 2. Particle image pairs in Ch1 and Ch2 with collocation traces, $R_{12,max}(t)$, with a median collocation value above a predefined threshold, $\tilde{R}_{12}$, are determined to be bound. Appropriate choices for median collocation thresholds are discussed in the following section.

To prevent highly correlated, nonparticle related events to contribute to bound event counts, we have also implemented an intensity-based threshold filter, which removes all collocated events with intensities 3 (for simulated) and 1 (for experimental data) standard deviation away from the mean of the "bound" particle population.

VALIDATION AND PERFORMANCE

Monte Carlo Simulations. We used Monte Carlo simulations, a well-accepted method of evaluating particle tracking algorithms,[23−28] to guide our choices of user specified algorithm parameters and to demonstrate the performance and robustness of our particle collocation algorithm. We first performed Monte Carlo simulations of Brownian particles with Gaussian brightness patterns of one pixel standard deviation (see SI Figure S.2 for example images). The particles were randomly distributed in a 500 × 150 cell simulation domain which corresponded to the pixel array. Particle diffusivity was set to 0.44 $\mu m^2/s$, and the particles were given a uniform advective velocity of $\vec{v}_{p,x}$ = 10 μm/s. As typical with Brownian Monte Carlo, we chose specular reflection boundary conditions for the side walls of the simulation domain. Further, particles exiting the x = 150 end of the domain were reintroduced at x = 0, at random y-coordinates. To explore the sensitivity of our method to experimental conditions, we simulated the following variations: (1) percentage of bound particles between the two channels ranged between 0 and 100%, (2) interparticle distance varied between 5 and 20 μm, and (3) image signal-to-noise ratio (SNR) ranged between 2 to 100. Note that the average interparticle distance of nearest neighbor particles in 2D can be determined as $L_{IP} = 0.5\eta^{-1/2}$ (see section S.4 in SI), where $\eta(m^{-2})$ is particle density. Interparticle distance of 5 to 20 μm is equivalent to about 800 to 50 particles in a 500 × 150 simulation domain.

Image SNR and Median Collocation Threshold. The probability of successful particle identification and collocation rely strictly on the degree of correlation between two normalized brightness patterns. Signal-to-noise ratio (SNR) has a strong effect on the brightness pattern of raw particle images. We define SNR as the peak particle intensity above the mean of local background divided by 2 times the standard deviation of background image intensity. To determine how SNR influences particle tracking and collocation accuracy, we added Gaussian white noise to the simulated particle fields (see SI Figure S.2 for simulated images with SNR of 2 and 100). During the 200 s simulation time, we introduced 1422 of unique particles, 1200 of which had a residence time of roughly 15 s. We performed particle tracking on the simulated images and plot in SI Figure S.2 the histogram of tracked particle times as a function of SNR. In the case of low image SNR (SNR = 2), over 200 s, approximately 5000 particles were identified, but only 10% were tracked for 3 s or longer (SI Figure S.2). Note, that when the algorithm loses a particle due to the interfering effects of SNR, if the same particle reemerges at a later time step, it is identified as a new particle (as would happen in an experiment). Consequently, the number of particle counts increases, and tracked particle times shorten with increasing image noise. Consistent with this is the large discrepancy present between the number of particles detected (∼5000) and simulated (∼1400) at SNR = 2. For image SNR of 5 or above, the number of particles identified and their tracked time converges to the known values.

In Figure 3, we show the combined accuracy of particle tracking and collocation as a function of SNR and collocation

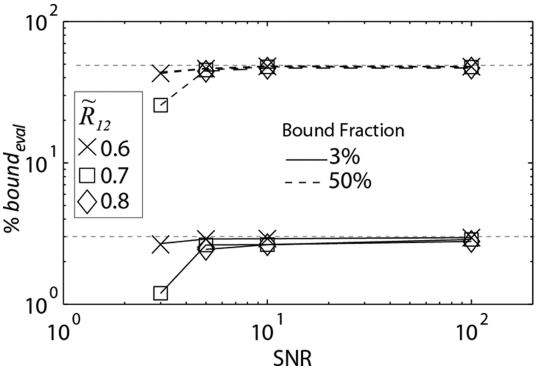

Figure 3. Accuracy of particle hybrid count as a function of simulated SNR and the median collocation threshold, $\tilde{R}_{12}$. The total number of 1 μm diameter particles in each image from the Monte Carlo simulation is 100 (with a mean interparticle distance of roughly 15 μm). The simulated fraction of bound versus total particle number was 3% (solid line) and 50% (dashed line). Particles were considered only if they were tracked for 10 s or longer. For the tested range of collocation thresholds, the bound particle fraction is underpredicted. For the highest collocation threshold of 0.8, PITC detected no bound particles for SNR < 5. As SNR increases above 5, the detected bound fraction converges to the simulated values.

median threshold, $\tilde{R}_{12}$ for two different simulation fractions of bound particles. For both cases of 3% and 50% bound particles, increasing image SNR improves collocation accuracy. In general, strong image noise results in an underestimation of the bound fraction. For SNR = 2, no bound particles were detected for any collocation thresholds in the tested range ($\tilde{R}_{12}$ = 0.6−0.8). The collocation results for images with SNR = 3, using threshold of $\tilde{R}_{12}$ = 0.6 are in close agreement with the simulated values, but raising $\tilde{R}_{12}$ to 0.8, causes complete failure of the collocation analysis. For SNR > 5, the collocation accuracy is weakly dependent on SNR and collocation thresholds. For example, prediction of PITC analysis of the 3% bound fraction case (solid line) at SNR = 10, is 2.91%, when $\tilde{R}_{12}$ = 0.6 and 2.64%, when $\tilde{R}_{12}$ = 0.7 − 0.8. On the basis of these analyses, we determined that a value of $\tilde{R}_{12}$ = 0.6 yields an appropriate accuracy for a fairly wide range of image SNR.

In the SI, we present results of collocation analyses performed with 0% simulated bound particle fraction (c.f. SI Figure S.3). We used such simulations to study the limit of detection (LOD) of our method in absence of bound particles and quantify false positive rates in negative controls. For example, at image SNR = 100, the PITC algorithm found that bound particle doublets made up 0.9%, 0.6%, and 0.25% of the total particles for collocation threshold values of 0.6, 0.7, and 0.8, respectively. After we performed a simple calibration of Ch2 particle intensities using PMC-PC, the PITC algorithm detected 0% bound fractions for all collocation thresholds in the negative control case. (See SI section S.6 for more details.)

Particle Density and Monitoring Time. The rate of particle analysis of our collocation method is primarily limited by two parameters, the maximum particle concentration tolerated by the PITC algorithm and the minimum monitoring

dx.doi.org/10.1021/ac402830q | Anal. Chem. XXXX, XXX, XXX−XXX

time, t_m. Here we examine the effect of these parameters on particle tracking and collocation performance. We analyzed image pairs containing 50, 100, 200, 400, and 800 particles per image, 3% of which were deterministically bound. During the 200 s simulation time, we introduced 718, 1437, 2851, 5692, and 11314 unique particles, most of which had a residence time (time spent in field of view) of roughly 15 s. In Figure S.2 of the SI, we show a histogram of tracked particle times (duration over which algorithm tracks each particle) as a function of particle density. At high particle density, neighboring particles can influence each other's brightness patterns, so the success rate of tracking and tracked particle times decrease. For image sets containing 200 or more particles, the tracked particle times are limited by particle crowding, and not by the user-specified parameters of velocity and interrogation widow-size. For example, for the highest particle density case (800 per image), most particles can be tracked for at most 5 s (c.f., SI Figure S.2).

In section S.7 of the SI, we present a detailed analysis of our algorithm's collocation performance as a function of the ratio of the interparticle distance, L_{IP}, to the characteristic distance that two randomly aligned particles must separate for the algorithm to consider them unbound, L_{ch} (eq 1). The latter includes a study of the influence of monitoring time, t_m on collocation by comparing t_m to the minimum elution time, t_{ch} (eq 2) (the characteristic time it takes two randomly bound particles to separate by L_{ch}). Briefly, at low particle densities (i.e., high L_{IP}/L_{ch}), random particle−particle interactions are rare, and the bound fractions detected by PITC converge to the simulated values for all t_m and $\tilde{R}_{12}$. For sufficiently high particles densities (L_{IP}/L_{ch} less than about 3.5), the data includes frequent random particle−particle interactions, and bound particle fractions for short observation times are overpredicted, as expected. In all cases, increasing monitoring time increases collocation certainty. For example, for values of $\tilde{R}_{12} = 0.7$, $t_m/t_{ch} = 3.87$ and $L_{IP}/L_{ch} > 3$, the algorithm measured values are within ~10% of the correct value for SNR = 100 (for the case of only 3% particles bound where bound fraction was estimated to be between 2.7% and 3.3%).

On the basis of the aforementioned study of the influence of L_{IP}/L_{ch}, we recommend using particle densities which yield approximately $L_{IP}/L_{ch} > 3$, and a collocation threshold of $\tilde{R}_{12} = 0.7$. We note that images with SNR of less than about 5 will likely require a slightly lower value of $\tilde{R}_{12}$ (say 0.6 or 0.65). In general, we recommend monitoring times of 2 times the minimum evolution time, t_{ch}, or higher.

EXPERIMENTAL DEMONSTRATION OF CYTOMETRY-LIKE DATA AND COLLOCATION ANALYSIS

We here show an experimental demonstration of our particle tracking and collocation method by analyzing a solution containing two populations of 1 μm diameter, fluorescent beads, and DNA targets of length 173 nt. Each bead population has a unique spectral signature and each is functionalized with unique molecules complementary to the target (21 nt sequences for both Ch1 and Ch2 beads). The DNA target and two probe sequences are listed in SI section S.9. Upon hybridization to the complementary oligos, the target DNA bridges the two beads, creating a two-color bead doublet (SI Figure S.5). The resulting bead solution containing three bead populations, red singlets, green singlets, and red-green bead hybrids, were loaded onto a microfluidic chip (SI Figure S.6) and imaged with our dual-view system. We also performed a negative control experiment, using bead suspension absent of the DNA target.

Time Resolved Collocation Coefficient. Monitoring collocation and other particle parameters in time improves the accuracy of our estimates, as many sources of variation are uncorrelated in time. One example of this is the discretization error associated with imaging with a CCD array. For instance, particle intensities can vary significantly depending on the location of their center relative to the pixel edge. Another source of variation is associated with the random interaction between particles which can cause "spikes" in the collocation coefficient, $R_{12,max}(t)$. Acquiring a single realization in time would therefore yield significant error in particle-to-particle binding studies. In Figure 4, we show this phenomenon by plotting the collocation coefficients evaluated from the experimentally obtained image sets. We set the minimum monitoring time to 8 s, which is approximately 3.2 times longer than the characteristic evolution time, t_{ch}, for this experiment. Filtering particles based on the 8 s of minimum monitoring time yielded time-resolved measurements of particle fluorescence, radius, and collocation for 163 red beads. The plot in the figure shows 50 representative traces of the time-resolved collocation coefficient, $R_{12,max}(t)$, for the red particles correlated with the green channel in the presence of DNA. The distribution of $R_{12,max}(t)$ for all realizations of the 163 red beads is shown on the right-hand side of Figure 4. To accurately determine the fraction of bound beads (two-color doublets), we set the median collocation threshold to 0.65 and filtered out particle matches with intensity lower than 1 standard deviation from the mean of green particle matches. The black shaded region of the PDF is associated with the bound and the gray shaded region is associated with the unbound beads. The appropriateness of this collocation threshold is corroborated by the distinct difference between the bound (solid) and unbound (dashed) collocation traces. Each of the bound traces has a high mean (and high median) value in time with a narrow variance, indicating deterministically correlated binding events. Meanwhile, the low mean (and low median) value and large variance of unbound collocation

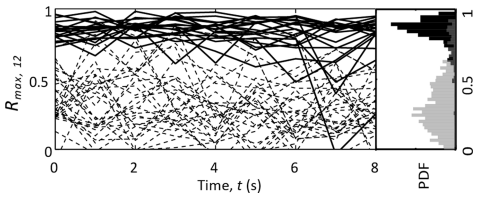

Figure 4. Measured normalized cross-covariance coefficients between Ch1 and Ch2 particle images of a bead suspension containing two sets of oligo-conjugated polystyrene beads (one red and one green) in the presence of complementary DNA. We here plot beads which were tracked for 8 s or longer. The plot shows 50 representative traces (20 of them were judged as bound by the algorithm). The PDF of the covariance coefficients are plotted on the right-hand side of the trace plot. The collocation traces of bound red beads remain relatively high during the 8 s of monitoring time, indicating deterministic interaction between Ch1 and Ch2 beads. This conclusion is supported by the high median (>0.8) and narrow variance of the collocation distribution plotted for the bound bead population. Conversely, the unbound traces reveal Gaussian-like distribution with broad variance and low mean collocation coefficient values (<0.3), suggesting rare, random bead−bead interactions.

dx.doi.org/10.1021/ac402830q | Anal. Chem. XXXX, XXX, XXX−XXX

traces indicate random, weakly correlated events, such as those associated with image noise or close proximity of a neighboring bead.

Cytometrylike Fluorescence Data. Integrated bead fluorescence were collected and analyzed to yield cytometry-like data. We identified and tracked beads in Ch1 and performed collocation analysis with Ch2 beads. The algorithm was then run again, but starting by identifying and tracking beads in Ch2 and collocating these with beads in Ch1. This process helps corroborate collocation information and helps reduce the effect of bead images which may fail threshold tests associated with particle tracking but not collocation analysis.

In Figure 5, we show the results of these two approaches overlaid on a scatter plot for two bead experiments (one negative control, and one containing target DNA). The fluorescence intensity of each bead was evaluated by integrating the intensity profile obtained from the nonlinear Gaussian fitting routine. In the PMC-PC phase, we set the size-based threshold to eliminate beads with radii larger than the mean plus 1 times the standard deviation of the bead population in each image. The intensity-based threshold eliminated all features with intensity 1 times the standard deviation away from the mean of the bead population.

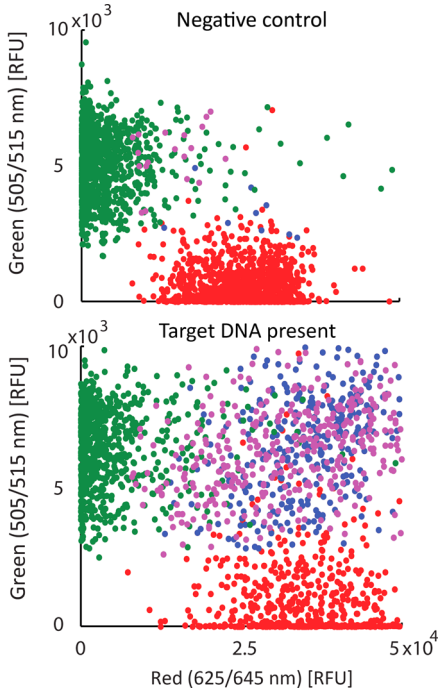

Figure 5. Multicolor bead hybrid fluorescence in a DNA-induced bead-to-bead binding assay. Algorithm parameters were set to $t_m/t_{ch} \cong 2$ and $\tilde{R}_{D,co} = 0.65$. Here we show overlaid results of two particle tracking approaches. In first approach, red beads were tracked and cross-correlated with green channel. In the second approach, green beads were tracked and cross-correlated with red channel. The green and red markers correspond to green and red fluorescent bead singlets. The purple subpopulations on the scatter plot represent the green beads that were judged by the algorithm as collocated with the red beads (G-R). The blue subpopulation was obtained with the second approach (R-G). When DNA is present in the bead suspension, 33% of red and 41% of green beads were judged as bound. In the absence of DNA, 0.8% of red and 1.6% of green beads were judged as deterministically bound.

By performing PITC analysis twice starting with alternate image channels, we obtained the intensity distribution of both Ch1 and Ch2 beads independently. These distributions were used to calibrate the intensity-based filters of the collocation phase.

We set the median threshold, $\tilde{R}_{12}$ to 0.65 and monitored the bead intensities and collocation for 5 s which is approximately 2 times longer than the characteristic evolution time, t_{ch}. In Figure 5, we plot the mean intensity of each bead. For the 200 s duration of this experiment, the PITC counted total of 7903 (1010) red and 9351 (1292) green beads in the DNA-containing solution, and 7641 (1127) red and 9966 (1163) green beads for the negative control solution. In parentheses, we note the number of beads that were tracked for 5 s or longer. In the solution containing DNA, the PITC algorithm detected 418 red beads collocated with green (R-G, blue markers), and 430 green beads collocated with red (G-R, purple markers).

In the negative control case, PITC detected 9 red beads collocated with green (R-G, blue markers), and 19 green beads collocated with red (G-R, purple markers). Visual inspection of the particle field revealed that a small fraction of beads did form two-color bead hybrids. We hypothesize that this is a result of DNA contamination and/or nonspecific bead-to-bead binding.

CONCLUDING REMARKS

We developed a custom algorithm which identifies particles, and tracks particle parameters including coordinate, size, intensity, and collocation with particle images in other wavelengths. We studied the effects of SNR and particle concentration on particle identification, tracking and collocation using Monte Carlo simulations. This analysis suggests that the optimum algorithm performance is achieved for SNR > 5 and interparticle distance of $L_{IP} > 3\ L_{ch}$. For particle-to-particle collocation we recommend analysis for sufficiently long durations of $t_m > 2\ t_{ch}$. We experimentally demonstrated the method by imaging randomly dispersed fluorescence beads electrophoretically driven through a microchannel. We induced bead-to-bead binding by functionalizing two sets of beads with DNA probes complementary to two respective sections of a common DNA target molecule. The assay identified thousands of unique beads and tracked over 1000 of these for longer than 5 s. Time-resolved tracking of these beads and collocation between two emission (optical) channels were used to detect the target molecule. In positive control experiments, over ~40% beads participated in bead-DNA-bead hybrids. In the negative control, the number of beads identified as collocated with another color was about 1%.

We optimized and demonstrated this method for challenging image data associated with particle-to-particle binding. However, we note that this method is equally applicable for assays where particles are not expected to interact or in cases where individual particles emit in two colors. For instance, we hypothesize that our method can be applied to simple and rapid cell-based diagnostics (e.g., TB and malaria)[1] or to two to four color immunophenotyping assays.[7] We hope to demonstrate size and fluorescence intensity analysis of cell suspensions with appropriate controls in future work.

Our assay uses off-the-shelf optics including a CCD camera, epifluorescence microscope, and color image splitter. We are able to analyze randomly distributed particles in situ as they travel within a variety of fluidic channels, provided the channels have optical access. Flow of particles can be induced by either

dx.doi.org/10.1021/ac402830q | Anal. Chem. XXXX, XXX, XXX–XXX

pressure-driven flow or electrophoresis to increase throughput of analysis. Our method can also obtain multiple spatially resolved images over finite times, so that it may be applicable to studying kinetic events such as on- and off-rates of particle-to-particle binding. Further, our method can analyze particle densities of 10^8 particles per milliliter (approximately 2 orders of magnitude greater than FCM techniques).

■ ASSOCIATED CONTENT

Supporting Information

Additonal material as described in the text. This material is available free of charge via the Internet at http://pubs.acs.org.

■ AUTHOR INFORMATION

Corresponding Author

*E-mail: juan.santiago@stanford.edu. Fax: 650-723-7657.

Notes

The authors declare no competing financial interest.

■ ACKNOWLEDGMENTS

A.R. was supported by a Sandia National Laboratories Campus Executive Graduate Research Project. Sandia Corporation (a wholly owned subsidiary of Lockheed Martin Corporation) is operator of Sandia National Laboratories under its U.S. Department of Energy Contract No. DE-AC04-94AL85000. The authors would like to thank Lewis A. Marshall for very helpful discussions, and providing constructive comments and valuable suggestions.

■ REFERENCES

(1) Shapiro, H. M.; Perlmutter, N. G. *Cytometry, Part B.* **2008**, *74* (S1), S152−S164.
(2) Tárnok, A.; Gerstner, A. O. *Cytometry* **2002**, *50* (3), 133−143.
(3) Wilson, R.; Cossins, A. R.; Spiller, D. G. *Angew. Chem., Int. Ed.* **2006**, *45* (37), 6104−6117.
(4) Ortiz, M. E.; Endy, D. *J. Biol. Eng.* **2012**, *6* (1), 1−12.
(5) Nam, J.-M.; Stoeva, S. I.; Mirkin, C. A. *J. Am. Chem. Soc.* **2004**, *126* (19), 5932−5933.
(6) Leslie, D. C.; et al. *J. Am. Chem. Soc.* **2012**, *134* (12), 5689−5696.
(7) De Rosa, S. C.; Brenchley, J. M.; Roederer, M. *Nat. Med.* **2003**, *9* (1), 112−117.
(8) Lenz, D.; Gerstner, A. O.; Laffers, W.; Steinbrecher, M.; Bootz, F.; Tarnok, A. *Proc. Biomed. Opt.* **2003**, 364−374.
(9) Shapiro, H. M. *Practical Flow Cytometry*, 4th ed.; Wiley-Liss: New York, 2003.
(10) Kamentsky, L. A.; Kamentsky, L. D. *Cytometry* **1991**, *12* (5), 381−387.
(11) Perfetto, S. P.; Chattopadhyay, P. K.; Roederer, M. *Nat. Rev. Immunol.* **2004**, *4* (8), 648−655.
(12) Quirke, P.; Dyson, J. *J. Pathol.* **1986**, *149* (2), 79−87.
(13) Brown, M.; Wittwer, C. *Clin. Chem.* **2000**, *46* (8), 1221−1229.
(14) Dunbar, S. A. *Clin. Chim. Acta* **2006**, *363* (1), 71−82.
(15) Zou, Y.; Heinemann, F. M.; Grosse-Wilde, H.; Sireci, G.; Wang, Z.; Lavingia, B.; Stastny, P. *Human Immunol.* **2006**, *67* (3), 230−237.
(16) Darzynkiewicz, Z.; Bedner, E.; Li, X.; Gorczyca, W.; Melamed, M. R. *Exp. Cell Res.* **1999**, *249* (1), 1−12.
(17) Kinosita, K.; Itoh, H.; Ishiwata, S.; Hirano, K.; Nishizaka, T.; Hayakawa, T. *J. Cell Biol.* **1991**, *115* (1), 67−73.
(18) Inagaki, T.; Arakawa, E.; Hamm, R.; Williams, M. *Phys. Rev. B* **1977**, *15* (6), 3243.
(19) Inoué, S. and Spring, K. R., *Video Microscopy: The Fundamentals (The Language of Science)*; Plenum: New York, 1997.
(20) Meinhart, C.; Wereley, S.; Gray, M. *Meas. Sci. Technol.* **2000**, *11* (6), 809.
(21) Chandrasekhar, S. *Rev. Mod. Phys.* **1943**, *15* (1), 1.
(22) Einstein, A. *Ann. Phys.* **1905**, *17* (549−560), 16.
(23) Adrian, R. J. and Westerweel, J. *Particle Image Velocimetry*; Cambridge University Press: Cambridge, U.K., 2010; Vol. *30*.
(24) Takehara, K.; Adrian, R. J.; Etoh, G. T.; Christensen, K. T. *Exp. Fluids* **2000**, *29* (1), S034−S041.
(25) Raffel, M.; Willert, C. E.; Wereley, S. T. and Kompenhans, J. *Particle Image Velocimetry—A Pratical Guide*, 2 ed.; Springer Press: Heidelberg, Germany, 2007.
(26) Keane, R.; Adrian, R.; Zhang, Y. *Meas. Sci. Technol.* **1995**, *6* (6), 754.
(27) Keane, R. D.; Adrian, R. J. *Meas. Sci. Technol.* **1990**, *1* (11), 1202.
(28) Westerweel, J. *Meas. Sci. Technol.* **1997**, *8* (12), 1379.